Hindawi
Journal of Robotics
Volume 2024, Article ID 9767914, 1 page
https://doi.org/10.1155/2024/9767914

Retraction

Retracted: Parameter-Tunable RBF Neural Network Control Facing Dual-Joint Manipulators

Journal of Robotics

Received 23 January 2024; Accepted 23 January 2024; Published 24 January 2024

This article has been retracted by Hindawi following an investigation undertaken by the publisher [1]. This investigation has uncovered evidence of one or more of the following indicators of systematic manipulation of the publication process:

(1) Discrepancies in scope
(2) Discrepancies in the description of the research reported
(3) Discrepancies between the availability of data and the research described
(4) Inappropriate citations
(5) Incoherent, meaningless and/or irrelevant content included in the article
(6) Manipulated or compromised peer review

The presence of these indicators undermines our confidence in the integrity of the article's content and we cannot, therefore, vouch for its reliability. Please note that this notice is intended solely to alert readers that the content of this article is unreliable. We have not investigated whether authors were aware of or involved in the systematic manipulation of the publication process.

Wiley and Hindawi regrets that the usual quality checks did not identify these issues before publication and have since put additional measures in place to safeguard research integrity.

We wish to credit our own Research Integrity and Research Publishing teams and anonymous and named external researchers and research integrity experts for contributing to this investigation.

The corresponding author, as the representative of all authors, has been given the opportunity to register their agreement or disagreement to this retraction. We have kept a record of any response received.

References

[1] W. Xu, "Parameter-Tunable RBF Neural Network Control Facing Dual-Joint Manipulators," *Journal of Robotics*, vol. 2022, Article ID 4231117, 10 pages, 2022.

Hindawi
Journal of Robotics
Volume 2022, Article ID 4231117, 10 pages
https://doi.org/10.1155/2022/4231117

Research Article

Parameter-Tunable RBF Neural Network Control Facing Dual-Joint Manipulators

Weiying Xu

HBUT Detroit Green Technology Institute, Hubei University of Technology, Wuhan 430000, China

Correspondence should be addressed to Weiying Xu; 2011611126@hbut.edu.cn

Received 8 July 2022; Revised 27 July 2022; Accepted 2 August 2022; Published 8 September 2022

Academic Editor: Shahid Hussain

In order to improve the parameter control effect of the double-joint manipulator, this paper combines the RBF neural network to control the parameters of the double-joint manipulator and the command filtering backstep impedance control method based on the RBF neural network is effectively applied to the multijoint manipulator. Moreover, this paper introduces the filter error compensation mechanism into the controller design to eliminate the influence caused by the filter error. Finally, the effectiveness and superiority of the command filtering backstep impedance control scheme of the multijoint manipulator adaptive neural network designed in this paper is verified by simulation experiments. The experimental research results verify that the parameter-tunable RBF neural network control method facing the dual-joint manipulator has a certain effect on the parameter control process of the dual-joint manipulator and can effectively improve the motion accuracy of the dual-joint manipulator.

1. Introduction

The theoretical modeling methods of robotic arms are generally based on the principle of energy conservation. For a rigid body, its energy usually includes two parts: kinetic energy due to motion inertia and potential energy due to gravitational field. However, for a flexible arm, its potential energy and kinetic energy are different from those of a rigid manipulator. Moreover, the flexible arm part generally includes three deformations, namely, rotational deformation, lateral deformation, and axial deformation [1]. In order to consider the bending deformation of beams, there are currently four basic modeling theories of beams [2]. Since the axial direction of the beam is generally longer than its diameter, the Euler–Bernoulli beam theory is generally used in many models. At the same time, since the flexible manipulator has infinite degrees of freedom, this is difficult to achieve in modeling. The general solution is to replace the infinite-dimensional degrees of freedom with finite-dimensional degrees of freedom and use Hamilton's principle or Lagrange dynamic equation to discretize a set of difference equations and finally solve them [3]. There are generally three current modeling methods for flexible manipulators [4]. The hypothetical mode method usually uses finite-dimensional continuous modes of several orders to represent infinite-dimensional beams. Moreover, each order mode is usually obtained by the product of the modal coordinates and the modal function, and finally, the consecutive several order modes are added to obtain the vibration amount at any point on the entire flexible arm. Literature [5] has demonstrated that the use of the second-order mode can accurately reflect the vibration offset of the flexible body. This research method has also been well verified experimentally and theoretically; however, this research method has certain deficiencies and cannot be applied to flexible manipulators with variable cross-sectional areas [6]. In response to this situation, some scholars have proposed the finite element method [7], and it has been shown that FE can reflect the actual situation well. For the lumped mass method, it is the simplest approximation to consider. It simply treats the flexible manipulator as a spring and mass system, but this research method is rarely used.

Traditional modeling of flexible arms generally chooses classical deformations to derive the Lagrangian dynamic equations of flexible arms. However, in some cases, this classical deformation does not conform to the actual

situation and cannot accurately describe the dynamic behavior of the flexible arm. For example, when the flexible arm rotates at a high speed, the comprehensive deformation theory can more accurately describe the deformation form of the flexible arm [8]. So far, in describing the elastic deformation of flexible arms, there are mainly three deformation descriptions: classical deformation theory, quadratic deformation theory, and comprehensive deformation theory. Classical deformation theory is currently the most widely used method [9]. Literature [10] uses the classical deformation theory to model the single-joint flexible manipulator and considers the influence of nonlinear centrifugal force on the accuracy of the model. Literature [11] uses the classical deformation theory to model a single-joint flexible manipulator and designs a controller based on this model, and the control effect is ideal. Literature [12] uses the classical deformation theory for modeling and then conducts positive feedback experiments and negative feedback experiments, respectively, and finally compares and analyzes the results of theoretical solutions and experiments. Analysis shows that positive feedback experiments are more robust than negative feedback in suppressing vibration. In addition, the end of the flexible manipulator contains a load to reduce the natural vibration frequency of the flexible manipulator. Literature [13] established the dynamic model of the Euler–Bernoulli beam using classical deformation theory and gave the numerical simulation results and concluded that the established dynamic model can be used as the control equation for the design and simulation of the control system. Literature [14] established a Lagrangian dynamic model of the flexible arm based on the assumed modal method and Lagrange equation through classical deformation theory and analyzed the physical and structural parameters and external driving torque of the flexible manipulator. It is concluded that these parameters will have an impact on the dynamic characteristics of the flexible manipulator. Literature [15] studied the theoretical modeling problem of two flexible manipulators in the plane and designed a controller based on the classical theoretical modeling problem. Literature [13] used the classical deformation method to study the kinematics of rigid-flexible coupled double rods in the plane and concluded that if the natural frequency of the first-order system of the flexible beam is lower than that of the natural frequency of the rigid beam, the frequency difference will increase with the increase in frequency. It increases with the increase in the natural frequency of the system; under the premise of certain initial conditions, the second-order natural frequency of the system will also increase with the increase in the natural frequency of the whole system, and it shows that the motion and deformation process of the manipulator will coordinate with each other when doing a large range of motion. There are mutual coupling characteristics.

When studying the control of the manipulator system, it is first necessary to study the dynamics modeling and kinematics analysis of the manipulator. As a theoretical basis for the study of the manipulator system, the dynamic modeling of the manipulator provides a dynamic model for the subsequent high-precision motion control of the manipulator end effector by making reasonable simplified assumptions for the actual manipulator system [16]. The kinematics analysis of the manipulator system is to establish the relationship between the manipulator joint variables and the end effector pose matrix by analyzing the two parts, including forward kinematics and inverse kinematics [17]. The positive kinematics issue is to obtain the pose matrix of the end effector by using the transformation matrix of the joint variables of the manipulator and inversely solving the value of each joint variable of the manipulator through various transformations. The inverse kinematics problem of the manipulator is the basis of the trajectory planning and trajectory tracking control of the joint end. However, in the process of inverse solution of the manipulator, multiple sets of solutions are often obtained. Therefore, it is necessary to select a set of suitable solutions according to the working conditions of the specific manipulator. Trajectory planning is another important direction of manipulator research. It is based on kinematics and dynamics analysis, according to the requirements of specific tasks, after a set of path points passed by the end effector of the manipulator is known, through the mechanical arm. The arm inverse solution is used to obtain the corresponding joint angle of each joint. Among them, the commonly used trajectory planning methods include cubic polynomial interpolation function, quintic polynomial interpolation function, and spline interpolation function [18]. In practical engineering applications, in order to ensure the smooth operation of each joint of the manipulator and to prevent the system from vibrating, the trajectory generated by the trajectory planning of the manipulator must be smooth and continuous and should have no sudden changes. The application of robotic arms in various industries is more extensive. It is not just a simple replacement for human work. In practical engineering, it puts forward higher requirements for its work execution efficiency and the control accuracy of end effectors. However, because the manipulator is a nonlinear, multiinput, multioutput system, when the system model is established, there are uncertain factors such as friction between joints, coupling, measurement error, and external disturbance. Therefore, reducing the influence of model uncertainty in the robotic arm system on the control accuracy of the end effector has always been a hot research topic in the field of control at home and abroad [19]. In recent years, with the development of the intelligent control theory, some advanced control theories have also been proposed. Although these advanced control theories can improve the tracking accuracy of the system to a certain extent, there are still some problems to be solved.

This paper combines the RBF neural network to control the parameters of the double-joint manipulator, improve the control effect of the two-joint manipulator, and promote the work efficiency of the manipulator.

2. Command Filtering Backstep Impedance Control of the Adaptive Neural Network for the Dual-Joint Manipulator

2.1. Command Filtering Backstep Impedance Control of Adaptive Neural Network. In recent years, to enable robots to handle increasingly complex tasks, many robots have installed dual-joint robotic arms with higher dexterity. When the robot provides services, the double-joint robotic arm will physically interact with the unknown external environment, so the compliance and safety of the double-joint robotic arm should be fully ensured to ensure the safety of physical interaction. To adjust the physical interaction force between the two-joint manipulator and the external environment, the impedance controller of the two-joint manipulator has been widely used in the interactive control of the robot.

At present, there have been many research achievements in the backstepping impedance controller of the double-joint manipulator. However, the "computational complexity" and "singularity" problems that may occur in the design process of the traditional backstepping method and the uncertain nonlinear terms in the dual-joint manipulator system due to the difficulty of obtaining the model parameters accurately deserve attention. In order to better solve these problems and make the dual-joint manipulator achieve better impedance control performance, this chapter introduces the adaptive neural network control technology into the design of the command filtering backstepping impedance controller. Moreover, this paper constructs an adaptive neural network command filtering backstep impedance controller for the dual-joint manipulator so that the uncertain dual-joint manipulator system can better realize the physical interaction control with the unknown external environment. Compared with the existing dual-joint manipulator control scheme, this control scheme has the following advantages:

The dynamic equation of the double-joint manipulator system can be described as follows:

$$D(x)\ddot{x} + C(x,\dot{x})\dot{x} + G(x) = u - \tau_e. \tag{1}$$

We define $x_1 = x$ and $x_2 = \dot{x}$, and the model of the double-joint robotic arm system can be rewritten in the following form:

$$\dot{x}_2 = D^{-1}(x_1)(u - \tau_e - C(x_1, x_2)x_2 + G(x_1)). \tag{2}$$

The command filter used in this chapter can be seen in formula (2). In order to improve the control accuracy of the dual-joint manipulator system, the compensation signal will be constructed to compensate for the filtering error generated by the command filter. The compensation signal design is as follows:

$$\begin{cases} \dot{\xi}_1 = -K_1\xi_1 + \xi_2 + (x_{1,c} - \alpha), \\ \dot{\xi}_2 = 0. \end{cases} \tag{3}$$

Among them, the control gain matrix is $K_1 = K_1^T > 0$ and x is the output signal vector of the filter. When $t = 0$, ξ_1 and ξ_2 are zero vectors.

The error variable is defined, where x_r is the tracking trajectory of the dual-joint manipulator through the impedance relationship. The design steps of the controller are as follows:

Step 1: the algorithm constructs the Lyapunov function as $V_1 = (1/2)v_1^T v_1$ and derives V_1 to get

$$\dot{V}_1 = v_1^T \dot{v}_1 = v_1^T(\dot{z}_1 - \dot{\xi}_1) = v_1^T(x_2 - \dot{x}_r - \dot{\xi}_1). \tag{4}$$

The virtual control law α is designed as

$$\alpha = -Kz_1 + \dot{x}_r. \tag{5}$$

Among them, the control gain matrix is $K_1 = K_1^T > 0$. By substituting formulas (3) and (5) into formula (4), we get

$$\dot{V}_1 = v_1^T(z_2 + x_{1,c} + \alpha - \alpha - \dot{x}_r - \dot{\xi}_1) = -v_1^T K_1 v_1 + v_1^T v_2. \tag{6}$$

Step 2: next, the algorithm selects the Lyapunov function as follows:

$$V_2 = V_1 + \frac{1}{2}v_2^T D(x_1)v_2. \tag{7}$$

The time derivative of the abovementioned formula is obtained as follows:

$$\begin{aligned} \dot{V}_2 &= \dot{V}_1 + v_2^T D(x_1)\dot{v}_2 + \frac{1}{2}v_2^T D(x_1)v_2, \\ &= v_2^T \begin{pmatrix} u - \tau_e - C(x_1, x_2)x_2 + v_1 \\ -G(x_1) - D(x_1)(\dot{x}_{1,c} + \dot{\xi}_2) \end{pmatrix} - v_1^T K_1 v_1 + \frac{1}{2}v_2^T \dot{D}(x_1)v_2. \end{aligned} \tag{8}$$

Since there are uncertain nonlinear terms in $D(x_1)$, $C(x_1, x_2)$ and $G(x_1)$, adaptive neural network techniques are used to approximate the matrix terms $D(x_1)$, $C(x_1, x_2)$, and $G(x_1)$.

The real control law u for designing a dual-joint robotic arm system is

$$u = -K_2 z_2 + \tau_e + \widehat{W}_D^T S_D(Z_D) x_{1,c} + \widehat{W}_C^T S_C(Z_C) x_{1,c} + \widehat{W}_G^T S_G(Z_G) - \nu_1 - K_r \text{sign}(\nu_2). \tag{9}$$

The neural network weight adaptation law is designed as

$$\dot{\widehat{W}}_{Dk} = -\Gamma_{Dk}\left(\sigma_{Dk}\widehat{W}_{Dk} + S_{Dk}(Z_D)\dot{x}_{1,c}\nu_{2k}\right), \tag{10}$$

$$\dot{\widehat{W}}_{Ck} = -\Gamma_{Ck}\left(\sigma_{Ck}\widehat{W}_{Ck} + S_{Ck}(Z_C)\dot{x}_{1,c}\nu_{2k}\right), \tag{11}$$

$$\dot{\widehat{W}}_{Gk} = -\Gamma_{Gk}\left(\sigma_{Gk}\widehat{W}_{Gk} + \phi_{Gk}(Z_G)\nu_{2k}\right). \tag{12}$$

Among them, the matrix is $\Gamma_{Dk} > 0, \Gamma_{Ck} > 0, \Gamma_{Gk} > 0$. $\sigma_{Dk}, \sigma_{Ck}, \sigma_{GFk}$ are all positive numbers to improve robustness.

$$W_D^{*T} S_D(Z_D) = D + \varepsilon_D, \tag{13}$$

$$W_C^{*T} S_C(Z_C) = C + \varepsilon_C, \tag{14}$$

$$W_G^{*T} S_G(Z_G) = G + \varepsilon_G. \tag{15}$$

Among them, ε_D, ε_C, and ε_G are minimal approximation error matrices.

$$\dot{V}_2 = -\nu_1^T K_1 \nu_1 - \nu_2^T K_2 \nu_2 + \nu_2^T \widetilde{W}_D^T S_D(Z_D)\dot{x}_{1,c} + \nu_2^T \widetilde{W}_C^T S_C(Z_C)\dot{x}_{1,c} + \nu_2^T \widetilde{W}_G^T S_G(Z_G) + \nu_2^T (E_r - K_r \text{sign}(\nu_2)). \tag{16}$$

Note 1: within the designed control law, the control parameter K_r should be selected as $K_{rii} \geq \|E_{ri}\|$. In order to ensure the stability of the method proposed in this chapter when the double-joint manipulator is working, a larger value of K_r should be selected, but this is also not the best way for the system to induce chattering. Therefore, the control parameter K_r should be changed to $K_r = k_D \dot{x}_{1,c} + k_c x_{1,c} + k_G$. Among them, $k_D \geq \|\varepsilon_D\|$, $k_C \geq \|\varepsilon_C\|$, and $k_G \geq \|\varepsilon_G\|$.

2.2. System Stability Analysis. In this section, the Lyapunov theorem will be used to determine the stability of the closed-loop system of the double-joint manipulator under the proposed control scheme. The Lyapunov function is selected as follows:

$$V = V_2 + \frac{1}{2}\sum_{k=1}^{n} \widetilde{W}_{Dk}^T \Gamma_{DK}^{-1} \widetilde{W}_{Dk}^T + \frac{1}{2}\sum_{k=1}^{n} \widetilde{W}_{Ck}^T \Gamma_{CK}^{-1} \widetilde{W}_{Ck}^T + \frac{1}{2}\sum_{k=1}^{n} \widetilde{W}_{Gk}^T \Gamma_{GK}^{-1} \widetilde{W}_{Gk}^T. \tag{17}$$

Substituting formulas (8) to (10) and (14) into the derivative of formula (15), we get

$$\begin{aligned}\dot{V} = {} & -\nu_1^T K_1 \nu_1 - \nu_2^T K_2 \nu_2 + \nu_2^T \widetilde{W}_D^T S_D(Z_D)\dot{x}_{1,c} + \nu_2^T \widetilde{W}_C^T S_C(Z_C)\dot{x}_{1,c} \\ & + \nu_2^T \widetilde{W}_G^T S_G(Z_G) + \nu_2^T (E_r - K_r \text{sign}(\nu_2)) \\ & - \sum_{k=1}^{n} \sigma_{DK} \widetilde{W}_{Dk}^T \widehat{W}_{Dk}^T - \sum_{k=1}^{n} \widetilde{W}_{Dk}^T S_{DK}(Z_D)\dot{x}_{1,c}\nu_{2k} \\ & - \sum_{k=1}^{n} \widetilde{W}_{Ck}^T S_{CK}(Z_C)\dot{x}_{1,c}\nu_{2k} - \sum_{k=1}^{n} \sigma_{CK} \widetilde{W}_{Ck}^T \widehat{W}_{Ck}^T - \sum_{k=1}^{n} \sigma_{GK} \widetilde{W}_{Gk}^T \widehat{W}_{Gk}^T \\ & - \sum_{k=1}^{n} \widetilde{W}_{Gk}^T S_{GK}(Z_G)\nu_{2k}.\end{aligned} \tag{18}$$

The following relation can be obtained as follows:

$$\nu_2^T \widetilde{W}_D^T S_D(Z_D)\dot{x}_{1,c} = \sum_{k=1}^{n} \widetilde{W}_{Dk}^T S_{Dk}(Z_D)\dot{x}_{1,c}\nu_{2k}, \tag{19}$$

$$\nu_2^T \widetilde{W}_C^T S_C(Z_C)\dot{x}_{1,c} = \sum_{k=1}^{n} \widetilde{W}_{Ck}^T S_{Ck}(Z_C)\dot{x}_{1,c}\nu_{2k}, \tag{20}$$

$$\nu_2^T \widetilde{W}_G^T S_G(Z_G) = \sum_{k=1}^{n} \widetilde{W}_{Gk}^T S_{Gk}(Z_G)\nu_{2k}. \tag{21}$$

Based on Young's inequality, the following formula can be obtained as

$$-\widetilde{W}_{Dk}^T \widehat{W}_{Dk}^T \leq -\frac{1}{2}\widetilde{W}_{Dk}^T \widetilde{W}_{Dk}^T + \frac{1}{2} W_{Dk}^{*T} W_{Dk}^*, \tag{22}$$

$$-\widetilde{W}_{Ck}^T \widehat{W}_{Ck}^T \leq -\frac{1}{2}\widetilde{W}_{Ck}^T \widetilde{W}_{Ck}^T + \frac{1}{2} W_{Ck}^{*T} W_{Ck}^*, \tag{23}$$

$$-\widetilde{W}_{Gk}^T \widehat{W}_{Gk}^T \leq -\frac{1}{2}\widetilde{W}_{Gk}^T \widetilde{W}_{Gk}^T + \frac{1}{2} W_{Gk}^{*T} W_{Gk}^*. \tag{24}$$

Substituting formulas (19) to (24) into formulas (18) and $K_{rii} \geq \|E_{ri}\|$, we get

$$\begin{aligned}\dot{V} \leq {} & -\nu_1^T K_1 \nu_1 - \nu_2^T K_2 \nu_2 - \frac{1}{2}\sum_{k=1}^{n} \sigma_{DK} \widetilde{W}_{Dk}^T \widehat{W}_{Dk}^T - \frac{1}{2}\sum_{k=1}^{n} \sigma_{CK} \widetilde{W}_{Ck}^T \widehat{W}_{Ck}^T \\ & - \frac{1}{2}\sum_{k=1}^{n} \sigma_{GK} \widetilde{W}_{Gk}^T \widehat{W}_{Gk}^T + \frac{1}{2}\sum_{k=1}^{n} \sigma_{DK} \widetilde{W}_{Dk}^{*T} \widehat{W}_{Dk}^* + \frac{1}{2}\sum_{k=1}^{n} \sigma_{CK} \widetilde{W}_{Dk}^{*T} \widehat{W}_{Ck}^* \\ & + \frac{1}{2}\sum_{k=1}^{n} \sigma_{GK} \widetilde{W}_{Gk}^{*T} \widehat{W}_{Gk}^* \\ \leq {} & a_0 V + c_0.\end{aligned} \tag{25}$$

From inequality (25), it can be deduced that all control signals of the closed-loop system of the double-joint manipulator are semiglobally uniformly asymptotically bounded. The design flow chart of the control method in this chapter can be seen in Figure 1:

Note 2: the size of the control parameter determines the radius of the tracking error domain. That is, the larger the control parameter $\lambda_{\max}(K_i)$, the smaller the radius of the tracking error domain.

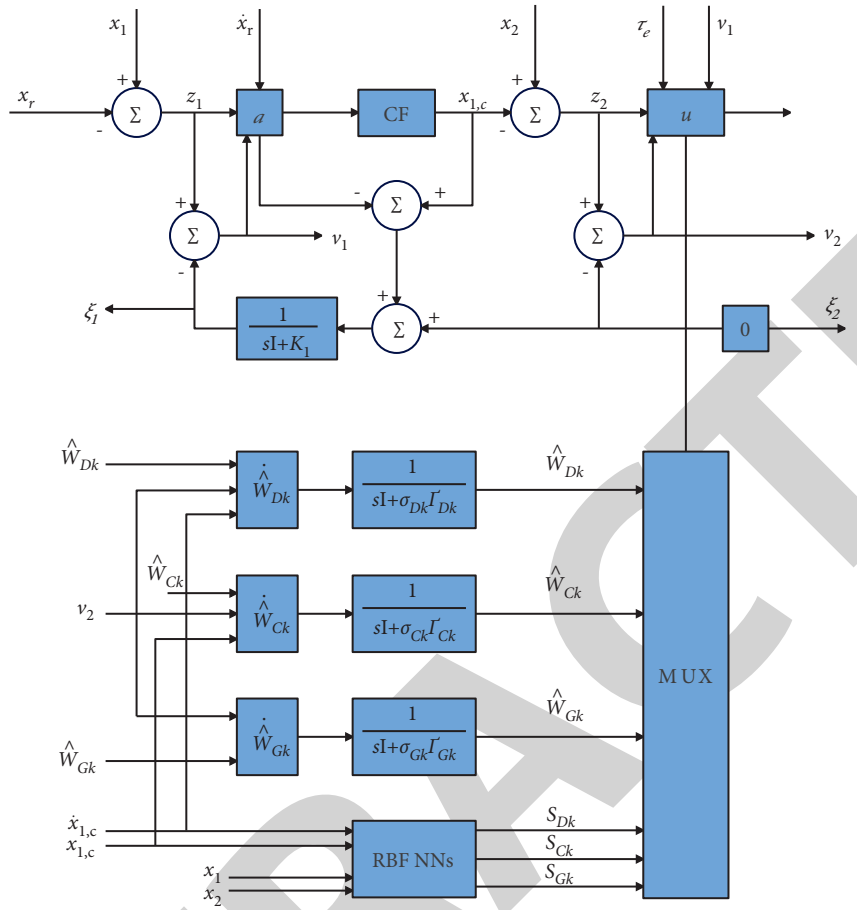

Figure 1: . Flowchart of the controller design.

Furthermore, through the integral inequality (25), we can get

$$V(t) \le V(0)e^{-a_0 t} + \frac{c_0}{a_0}\left(1 - e^{-a_0 t}\right) \le V(0) + \frac{c_0}{a_0}. \tag{26}$$

From the abovementioned inequality, we derive

$$\frac{1}{2}\left\|v_1(t)\right\|^2 \le V(0) + \frac{c_0}{a_0}. \tag{27}$$

From the abovementioned inequality, it can be known that, under the condition that all state quantities of the dual-joint manipulator system can be measured, for the initial compact set, $(v_1(0), v_2(0), \tilde{W}_{DK}(0), \tilde{W}_{CK}(0), \tilde{W}_{GK}(0)) \in \Omega_0$, $v_1(t)$ converges into the compact set Ω_{v_1}. By the same method, $v_2(t)$ can be converged into the compact set Ω_{v_2}, and $\tilde{W}_{DK}(0), \tilde{W}_{CK}(0), \tilde{W}_{GK}(0)$ can be converged into $\Omega_{\overline{W}_{Dk}}$, $\Omega_{\overline{W}_{Ck}}$, and $\Omega_{\overline{W}_{Gk}}$, respectively.

$$\begin{aligned}
\Omega_{v_1} &= \left\{ v_1(t) \in R^n \middle| \left\|v_1(t)\right\| \le \sqrt{2\left(V(0) + \left(c_0/a_0\right)\right)} \right\},\\
\Omega_{v_2} &= \left\{ v_2(t) \in R^n \middle| \left\|v_2(t)\right\| \le \sqrt{\frac{2\left(V(0) + \left(c_0/a_0\right)\right)}{\lambda_{\min}\left(D\left(x_1\right)\right)}} \right\},\\
\Omega_{\overline{W}_{Dk}} &= \left\{ \tilde{W}_{DK}(t) \in R^h \middle| \left\|v_2(t)\right\| \le \sqrt{\frac{2\left(V(0) + \left(c_0/a_0\right)\right)}{\lambda_{\min}\left(\Gamma_{Dk}^{-1}\right)}} \right\},\\
\Omega_{\overline{W}_{Ck}} &= \left\{ \tilde{W}_{CK}(t) \in R^h \middle| \left\|v_2(t)\right\| \le \sqrt{\frac{2\left(V(0) + \left(c_0/a_0\right)\right)}{\lambda_{\min}\left(\Gamma_{Ck}^{-1}\right)}} \right\},\\
\Omega_{\overline{W}_{Gk}} &= \left\{ \tilde{W}_{GK}(t) \in R^h \middle| \left\|v_2(t)\right\| \le \sqrt{\frac{2\left(V(0) + \left(c_0/a_0\right)\right)}{\lambda_{\min}\left(\Gamma_{Gk}^{-1}\right)}} \right\}.
\end{aligned} \tag{28}$$

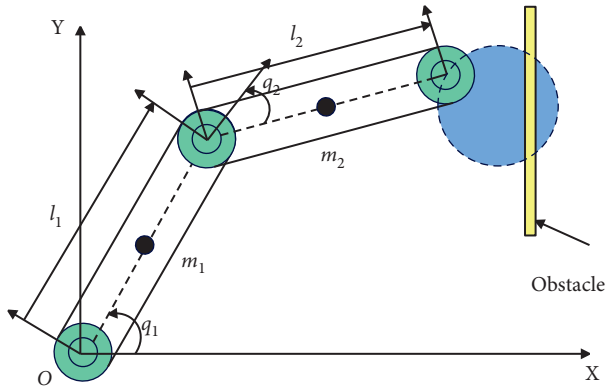

Figure 2: Plane two-joint robotic arm model.

From inequality (27), $\lim_{t\to\infty} \|v_1(t)\| \le \sqrt{2(c_0/a_0)}$ is easy to obtain. That is, for any given constant u, $\sqrt{2(c_0/a_0)} \le \mu$ can be obtained by adjusting the parameters a_0 and c_0, and thus, $\lim_{t\longrightarrow\infty} \|v_1(t)\| \le \mu$ can be obtained.

Note 3: increasing α_0 or decreasing c can effectively reduce $\sqrt{2(c_0/a_0)}$. Therefore, selecting a larger parameter a_0 can make the system obtain a sufficiently small tracking error of 0. However, because the parameters α and c both contain the parameter $\sigma_{Dk}, \sigma_{Ck}, \sigma_{Gk}\,(k = 1, 2, \ldots, n)$, the best control performance of the system requires the designer to accumulate experience in simulation research.

3. Analysis of Simulation Results

As shown in Figure 2, it is used for simulation experiments.

The model of the planar two-joint manipulator system used in this chapter is as follows:

$$\begin{cases} \dot{x}_2 = D^{-1}(x_1)[u - \tau_e - C(x_1, x_2)x_2 - G(x_1)], \\ y = x_1. \end{cases} \tag{29}$$

Here, $x_1 = [x_{11}, x_{12}]^T$ and $x_2 = [\dot{x}_{11}, \dot{x}_{12}]^T$. Among them, the connecting rod used in this simulation is a uniform and regular cuboid rod; then, there is $l_{ci} = (l_i/2)$.

According to the physical model of the two-joint manipulator, its kinetic energy equation can be calculated as

$$K(q, \dot{q}) = \frac{1}{2}m_1 l_{c1}^2 \dot{q}_1^2 + \frac{1}{2}I_1 \dot{q}_1^2 + \frac{1}{2}m_2 l_1^2 \dot{q}_1^2 + m_2 l_1 l_{c2} \dot{q}_1 (\dot{q}_1 + \dot{q}_2)\cos \dot{q}_2 + \frac{1}{2}m_2 l_{c2}^2 (\dot{q}_1 + \dot{q}_2) + \frac{1}{2}I_2 (\dot{q}_1 + \dot{q}_2)^2. \tag{30}$$

The potential energy of the two-joint manipulator can be expressed as

$$P(q) = m_1 g l_{C2} \sin q_1 + m_2 g[l_1 \sin q_1 + l_{c2} \sin(q_1 + q_2)]. \tag{31}$$

According to the Euler–Lagrange equation $d/dt\partial(K - P)/\partial\dot{q} - \partial(K - P)/\partial q = 0$, the inertia matrix $D(q)$ of the two-joint manipulator in the joint coordinate system, the centrifugal force and Coriolis force matrix $C(q, \dot{q})$, the gravity term matrix $G(q)$, and the Jacobian matrix of the two-joint manipulator in the joint coordinate system are expressed as

$$D(q) = \begin{bmatrix} m_1 l_{c1}^2 + m_2 l_1^2 + 2 l_1 l_{c2} \cos q_2 + I_1 + I_2, & m_2\left(l_{c2}^2 + l_1 l_{c2} \cos q_2\right) + I_2, \\ m_2\left(l_{c2}^2 + l_1 l_{c2} \cos q_2\right) + I_2, & m_2 l_{c2}^2 + I_2. \end{bmatrix}, \tag{32}$$

$$C(q, \dot{q}) = \begin{bmatrix} -m_2 l_1 l_{c2} \dot{q}_2 \sin q_2, & -m_2 l_1 l_{c2} (\dot{q}_1 + \dot{q}_2)_2 \sin q_{22}, \\ m_2 l_1 l_{c2} \dot{q}_1 \sin q_2, & 0. \end{bmatrix}, \tag{33}$$

$$G(q) = \begin{bmatrix} (m_1 l_{c2} + m_2 l_1) g \cos q_1 + m_2 l_{c2} g \cos(q_1 + q_2) \\ m_2 l_{c2} g \cos(q_1 + q_2). \end{bmatrix}, \tag{34}$$

$$G(q) = \begin{bmatrix} -(l_1 \sin q_1 + l_2 \sin(q_1 + q_2)), & -l_2 \sin(q_1 + q_2), \\ l_1 \cos q_1 + l_2 \cos(q_1 + q_2), & l_2 \cos(q_1 + q_2). \end{bmatrix}. \tag{35}$$

We assume that the initial position of the two-joint manipulator in Cartesian coordinates is selected as $x_{11}(0) = 0.5\,\text{m}$ and $x_{12}(0) = 0.8\,\text{m}$. In order to verify the effectiveness of the designed robot arm impedance method, an obstacle is set at the position of $x0 = 0.8\,\text{m}$ to obtain two-joint mechanical desired impedance parameters.

In order to more convincingly verify the effectiveness of the proposed command filter backstep impedance control method of the adaptive neural network, the model-based command filter impedance control method and the adaptive neural network dynamic surface backstepping impedance control are also used in the two-joint manipulator simulation experiment for comparative analysis. The gain

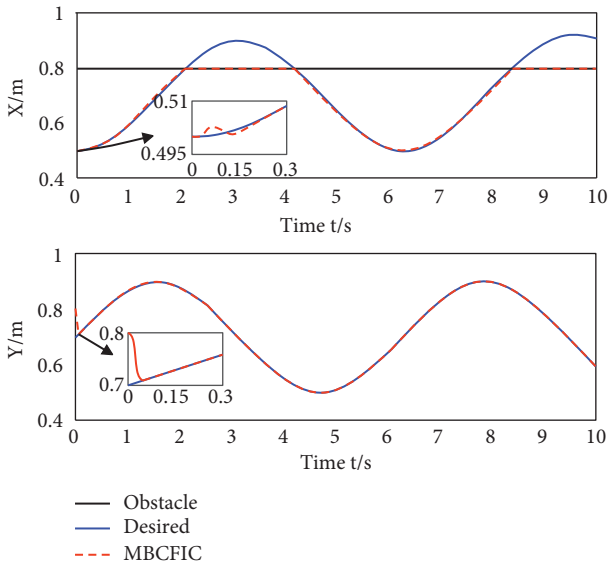

Figure 3: Position tracking curve (the model-based control method).

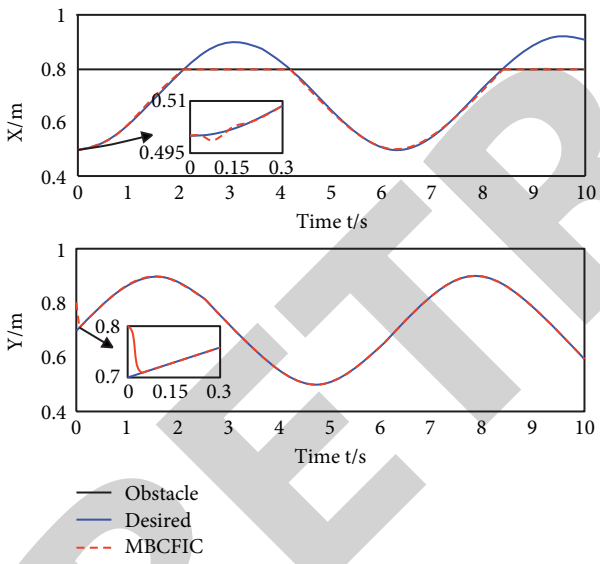

Figure 4: Position tracking curve (the command filtering method).

parameters of the three manipulator impedance control methods are selected as follows:

Method 1: for the model-based command filter impedance control (MBCFIC) method, the control law of the control method is designed as $u = -K_2 z_2 + \tau_e + D(x_1)\dot{x}_{1,c} + C(x_1, x_2)x_{1,c} + G(x_1) - v_1$. The control gain parameters are chosen as $K_1 = \text{diag}[50, 50]$ and $K_2 = \text{diag}[50, 50]$.

Method 2: for the adaptive neural network command filtering backstep impedance control (ANNCFIC) method, the center point of the RBF neural network in this paper is selected as $[-1, 1] < [-1, 1] \times [-1, 1] * [-1, 1] \times [-1, 1] \times [-11] * [-1, 1] * [-11] \times [-1, 1] \times [-1, 1]$. The initial weight of the RBF neural network is set to 0, and its adaptive law parameters are selected as $\Gamma_{DK} = \Gamma_{CK} = \Gamma_{GK} = \text{diag}[50, 50]$ and $\sigma_{DK} = \sigma_{CK} = \sigma_{GK} = 0.01$. The command filter parameters are selected as $w_n = 300$ and $g_n = 0.5$, and the control gain parameters are selected as $K_1 = \text{diag}[50, 50]$ and $K_2 = \text{diag}[50, 50]$.

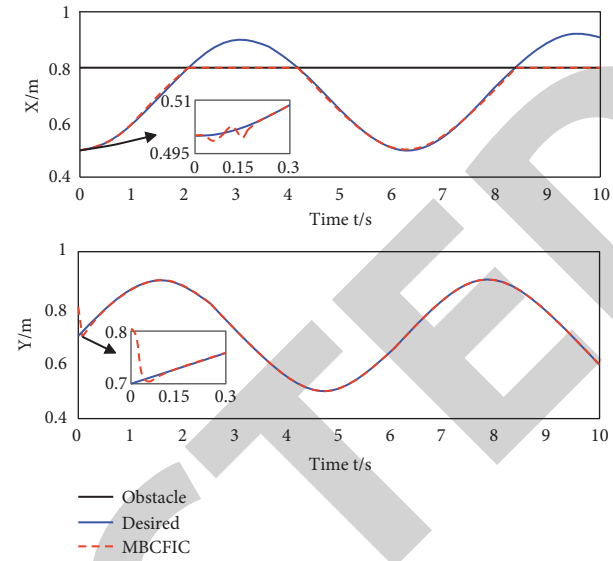

Figure 5: Position tracking curve (the dynamic surface method).

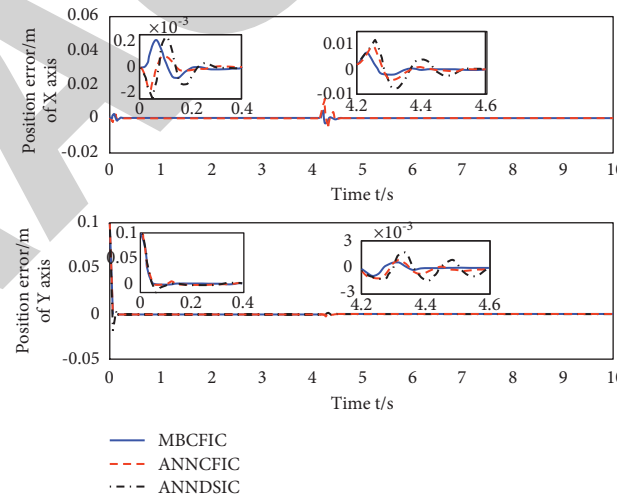

Figure 6: Comparison of position tracking errors of three control schemes.

Method 3: for the adaptive neural network dynamic surface backstepping impedance control (ANNDSIC) strategy, the dynamic surface used in this strategy is selected as $T\dot{\alpha}_d + \alpha_d = \alpha$ (T is a positive number). Therefore, the real control law of the control strategy is set to $u = -K_2 z_2 + \tau_e + \widehat{W}_D^T S_D(Z_D) \quad (\alpha - \alpha_d/T) \dot{x}_{1,c} + \widehat{W}_C^T S_C(Z_C)\alpha + \widehat{W}_G^T S_G(Z_G) - K\text{sign}(v_2)$, and the neural network structure and parameter selection are consistent with method 1. The control gain parameters

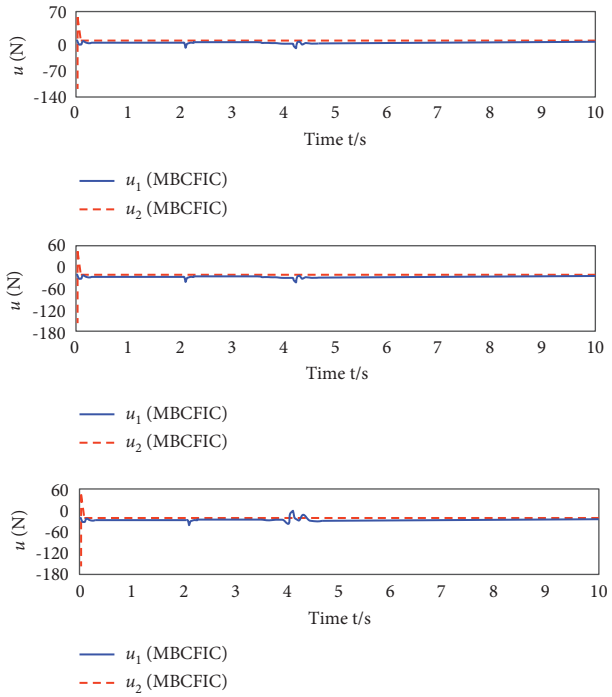

Figure 7: Control input curves of three control schemes.

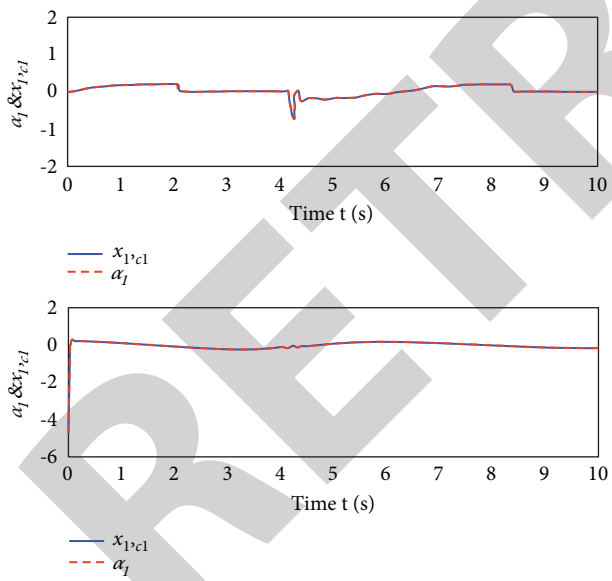

Figure 8: Curves of α and $x_{1,c}$.

are selected as $K_1 = \text{diag}[50, 50]$ and $K_2 = \text{diag}[50, 50]$, and the dynamic surface control parameters are selected as $T = 0.01$.

Figures 3–6 show the position tracking diagrams obtained from the simulation experiments of the three schemes. 3 to 5 are the position tracking curves of the model-based command filter impedance control method, the

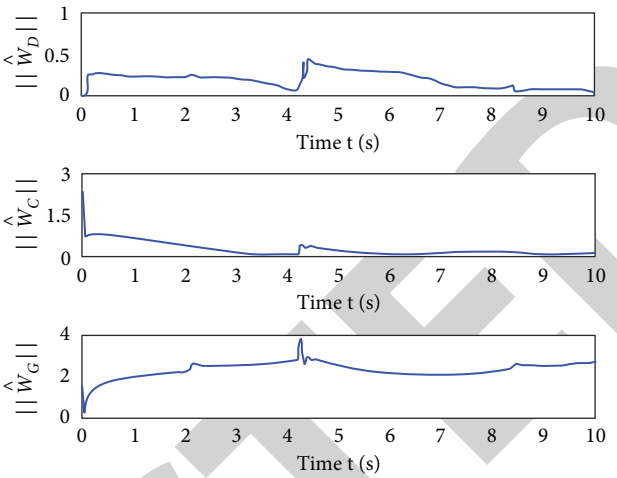

Figure 9: Neural network weight estimation curve for the proposed control scheme.

Table 1: Statistical table of the motion error of robotic arm.

Num	Error ratio
1	0.0431
2	0.0458
3	0.0305
4	0.0479
5	0.0030
6	0.0387
7	0.0218
8	0.0105
9	0.0262
10	0.0397
11	0.0361
12	0.0197
13	0.0053
14	0.0161
15	0.0330
16	0.0455
17	0.0378
18	0.0223
19	0.0286
20	0.0317
21	0.0270
22	0.0268
23	0.0196
24	0.0420
25	0.0195
26	0.0316
27	0.0415
28	0.0267
29	0.0407
30	0.0093
31	0.0196
32	0.0367
33	0.0406
34	0.0428
35	0.0393
36	0.0386

adaptive neural network command filter backstep

impedance control method, and the adaptive neural network dynamic surface backstep impedance control method, respectively. Figure 6 is a comparison diagram of the position tracking errors of these three control strategies. It can be seen from Figures 3 and 4 that the proposed neural network control method can achieve a good position tracking effect when the dynamic model of the manipulator is difficult to obtain accurately. This effectively proves that the adaptive neural network control can better approximate the uncertain nonlinear terms in the system. It can be seen from Figures 4 and 5 that the command filtering method used in this section has a smaller tracking error than the dynamic surface method. This proves that the designed error compensation mechanism can effectively eliminate the filtering error, which is beneficial for the robotic arm to be better applied to tasks with high tracking accuracy. It can be seen from Figure 6 that the proposed neural network command filter impedance control method has a good position tracking performance whether it is in contact with external obstacles or not.

Figure 7 shows a graph of the control input of the three control methods. It can be seen from the graph that the control input of the manipulator is kept within an appropriate range. Furthermore, it can be seen from Figure 8 that when the end effector of the robotic arm comes in contact with an external obstacle, a contact collision force is initially generated, but the impedance relationship can be quickly used to keep the contact force in a suitable range. Therefore, the proposed filtering can quickly realize impedance control, so that the end of the manipulator has a relatively safe physical interaction force when it contacts the external unknown environment. This proves that the proposed control method can effectively guarantee the safety of the manipulator when it is in contact with an unknown external environment. It can be seen from Figure 9 that the estimated value of the neural network weight of the control method proposed in this chapter is bounded. Through the comparative analysis of the above three control schemes, it can be proved that the designed adaptive neural network command filtering backstep impedance control method for the dual-joint manipulator system can effectively solve the problem that the dynamic model of the manipulator is difficult to obtain accurately. Moreover, it enables the robot arm to obtain a good position tracking effect and impedance tracking performance, ensuring the safety of the robot arm in contact with the unknown external environment.

The abovementioned research study verifies that the parameter-tunable RBF neural network control method for the dual-joint manipulator has certain effects on the parameter control process of the dual-joint manipulator. On this basis, through the simulation of multiple sets of data, the motion error of the manipulator is calculated, and the results shown in Table 1 are obtained.

It can be seen from the abovementioned research study that the parameter-tunable RBF neural network control method facing the double-joint manipulator can effectively improve the motion accuracy of the double-joint manipulator.

4. Conclusion

The force/position control of the double-joint manipulator system has become the general trend. The impedance control strategy of the double-joint manipulator treats the force control and the position control as a unified whole. Compared with other current multijoint manipulator force/position control methods, this method has very significant advantages. In the process of actual use, the amount of calculation is relatively small, and it has good robustness to changes in the external unknown environment. To achieve good impedance control of a multijoint manipulator, its end effector needs to have good position tracking performance. However, the multijoint manipulator is a highly nonlinear system with strong coupling effect which makes it difficult to construct the system model accurately, and also there are many unknown external disturbances. This paper combines the RBF neural network to control the parameters of the double-joint manipulator to improve the control effect of the two-joint manipulator and promote the work efficiency of the manipulator. The experimental study verifies that the parameter-tunable RBF neural network control method facing the double-joint manipulator has a certain effect on the parameter control process of the double-joint manipulator. Moreover, the parameter-tunable RBF neural network control method facing the double-joint manipulator can effectively improve the motion accuracy of the double-joint manipulator.

Data Availability

The labeled dataset used to support the findings of this study is available from the corresponding author upon request.

Conflicts of Interest

The author declares that there are no conflicts of interest.

Acknowledgments

This work was supported by Hubei University of Technology.

References

[1] Z. Xin, X. Wenbo, and L. Wenru, "The control strategy of manipulator based on fractional-order iterative learning," *Automatic Control and Computer Sciences*, vol. 55, no. 4, pp. 368–376, 2021.

[2] M. Bugday and M. Karali, "Design optimization of industrial robot arm to minimize redundant weight," *Engineering Science and Technology, an International Journal*, vol. 22, no. 1, pp. 346–352, 2019.

[3] S. Phukan and C. Mahanta, "A position synchronization controller for co-ordinated links (COOL) dual robot arm based on integral sliding mode: design and experimental validation," *International Journal of Automation and Computing*, vol. 18, no. 1, pp. 110–123, 2021.

[4] K. Morales, C. Hoyos, and J. M. García, "Mechanical structure design and optimization of a hu-manoid robot arm for education," *Journal of Autonomous Intelligence*, vol. 5, no. 1, pp. 95–109, 2022.
[5] J. K. Min, D. W. Kim, and J. B. Song, "A wall-mounted robot arm equipped with a 4-DOF yaw-pitch-yaw-pitch counterbalance mechanism," *IEEE Robotics and Automation Letters*, vol. 5, no. 3, pp. 3768–3774, 2020.
[6] S. Mori, K. Tanaka, S. Nishikawa, R. Niiyama, and Y. Kuniyoshi, "High-speed and lightweight humanoid robot arm for a skillful badminton robot," *IEEE Robotics and Automation Letters*, vol. 3, no. 3, pp. 1727–1734, 2018.
[7] D. Sáenz Zamarrón, N. I. Arana de las Casas, E. García Grajeda, J. F. Alatorre Ávila, and J. U. Naciff Arroyo, "Educational robot arm development," *Computación Y Sistemas*, vol. 24, no. 4, pp. 1387–1401, 2020.
[8] H. Fu and C. Ma, "Asynchronous resource-aware control for uncertain semi-Markov jump systems with application to robot arm," *Optimal Control Applications and Methods*, vol. 43, no. 3, pp. 925–942, 2022.
[9] M. Mukhtar, D. Khudher, and T. Kalganova, "A control structure for ambidextrous robot arm based on Multiple Adaptive Neuro-Fuzzy Inference System," *IET Control Theory & Applications*, vol. 15, no. 11, pp. 1518–1532, 2021.
[10] A. Hitzmann, H. Masuda, S. Ikemoto, and K. Hosoda, "Anthropomorphic musculoskeletal 10 degrees-of-freedom robot arm driven by pneumatic artificial muscles," *Advanced Robotics*, vol. 32, no. 15, pp. 865–878, 2018.
[11] H. H. Olewi, "Design and implementation of haptic robot arm," *Association of Arab Universities Journal of Engineering Sciences*, vol. 25, no. 5, pp. 256–268, 2018.
[12] F. Xu, H. Wang, K. W. S. Au, W. Chen, and Y. Miao, "Underwater dynamic modeling for a cable-driven soft robot arm," *IEEE/ASME transactions on Mechatronics*, vol. 23, no. 6, pp. 2726–2738, 2018.
[13] N. M. Ghaleb and A. A. Aly, "Modeling and control of 2-DOF robot arm," *International Journal of Emerging Engineering Research and Technology*, vol. 6, no. 11, pp. 24–31, 2018.
[14] W. S. Pambudi, E. Alfianto, A. Rachman, and D. P. Hapsari, "Simulation design of trajectory planning robot manipulator," *Bulletin of Electrical Engineering and Informatics*, vol. 8, no. 1, pp. 196–205, 2019.
[15] H. Yang, M. Xu, W. Li, and S. Zhang, "Design and implementation of a soft robotic arm driven by SMA coils," *IEEE Transactions on Industrial Electronics*, vol. 66, no. 8, pp. 6108–6116, 2019.
[16] K. Kunal, A. Z. Arfianto, J. E. Poetro, F. Waseel, and R. A. Atmoko, "Accelerometer implementation as feedback on 5 degree of freedom arm robot," *Journal of Robotics and Control (JRC)*, vol. 1, no. 1, pp. 31–34, 2020.
[17] M. Giuliani, D. Szczęśniak-Stańczyk, N. Mirnig et al., "User-centred design and evaluation of a tele-operated echocardiography robot," *Health Technology*, vol. 10, no. 3, pp. 649–665, 2020.
[18] X. Liang, H. Cheong, Y. Sun, J. Guo, C. K. Chui, and C. H. Yeow, "Design, characterization, and implementation of a two-DOF fabric-based soft robotic arm," *IEEE Robotics and Automation Letters*, vol. 3, no. 3, pp. 2702–2709, 2018.
[19] V. D. Cong, "Industrial robot arm controller based on programmable System-on-Chip device," *FME Transactions*, vol. 49, no. 4, pp. 1025–1034, 2021.